

DOES THE 62-DAY X-RAY PERIODICITY COME FROM ULX M82 X-1?

YANLI QIU^{1,2}, JIFENG LIU^{†1}, JINCHENG GUO^{1,2} AND JING WANG³

Draft version June 12, 2018

ABSTRACT

M82 X-1 is the brightest ultraluminous X-ray source in starburst galaxy M82 and is one of the best intermediate mass black hole candidates. Previous studies based on the *Rossi X-ray Timing Explorer* /Proportional Counter Array (*RXTE*/PCA) reported a regular X-ray flux modulation of M82 with a period of 62 days, and attributed this periodic modulation to M82 X-1. However, this modulation is not necessarily from M82 X-1 because *RXTE*/PCA has a very poor spatial resolution of $\sim 1^\circ$. In this work, we analyzed 1000 days of monitoring data of M82 X-1 from the *Swift*/X-ray telescope (XRT), which has a much better spatial resolution than *RXTE*/PCA. The periodicity distribution map of M82 reveals that the 62-day periodicity is most likely not from M82 X-1, but from the summed contributions of several periodic X-ray sources $4''$ southeast of M82 X-1. However, *Swift*/XRT is not able to resolve those periodic sources and locate the precise origin of the periodicity of M82. Thus, more long-term observations with higher spatial resolution are required.

Subject headings: galaxies: individual (M82) — X-rays: binaries

1. INTRODUCTION

Ultraluminous X-ray sources (ULXs; Fabbiano 2006) discovered in other galaxies exhibit high X-ray luminosities $L_X \geq 2 \times 10^{39}$ erg s^{-1} , and are possibly the long sought after intermediate mass black holes (IMBHs) radiating at sub-Eddington levels. Recent studies have shown that, except for a few cases, many ULXs can be stellar mass black holes in an ultraluminous state under supercritical accretion (Gladstone & Roberts 2009). Indeed, optical monitoring campaigns of two ULXs, M101 ULX-1 (Liu et al. 2013) and NGC 7793 P13 (Motch et al. 2014), have confirmed both to be stellar mass black holes, while *NuSTAR* observations of M82 have discovered that a transient ULX, M82 X-2, is actually powered by an accreting neutron star (Bachetti et al. 2014).

M82 X-1 (CXO J095550.2+694047) is the brightest ULX in the starburst galaxy, M82, at a distance of 3.6Mpc (Freedman et al. 1994), and arguably the best IMBH candidate in the local universe. M82 X-1 exhibits extremely high luminosities that can reach 10^{41} erg s^{-1} in the 0.5 – 10 keV bands (Kaaret et al. 2001; Matsumoto et al. 2001; Kaaret et al. 2009), suggesting an IMBH of about $10^3 M_\odot$ if radiating at the Eddington level. Recently, Pasham et al. (2014) re-analyzed 6-year *Rossi X-ray Timing Explorer* (*RXTE*) X-ray observations and revealed the high-frequency, 3:2 ratio, twin-peak quasi-periodic oscillations (QPOs) of 3.3 Hz and 5Hz, which, in combination with the low-frequency QPO revealed by an *XMM-Newton* observation, suggests an IMBH of $415 \pm 63 M_\odot$ under the relativistic precession model (Motta et al. 2014).

Interestingly, X-ray observations of M82 with the Pro-

portional Counter Array (PCA) on board *RXTE* over eight months has revealed regular modulations of about 20% with a period of about 62 days (Kaaret et al. 2006; Kaaret & Feng 2007, hereafter KF07). Kaaret et al. (2006) interpreted such a period as the orbital period for M82 X-1, and consequently derived a giant or supergiant companion for M82 X-1. However, the analysis of another 4.5-year *RXTE*/PCA light curve of M82 has shown a sudden phase shift of the 62-day modulation, suggesting the 62-day X-ray period may be caused by a precessing accretion disk around the black hole (Pasham & Strohmayer 2013, hereafter PS13).

While previous studies have attributed the periodic modulations in the *RXTE*/PCA light curves to M82 X-1, the brightest X-ray source in M82, it is not necessarily true because *RXTE*/PCA has a very poor spatial resolution of $\sim 1^\circ$, and the flux includes contributions from all X-ray sources in M82 ($11' \times 4'$) and nearby galaxies. In contrast, the X-ray telescope (XRT) on board the *Swift* satellite has a much better spatial resolution with a half power diameter of $18''$, and may resolve the bright point sources in M82. In this Letter, we use *Swift*/XRT observations over 1000 days to scrutinize the X-ray periodicity of M82. The data analysis and results are presented in §2, and the discussion follows in §3.

2. DATA ANALYSIS AND RESULTS

The *Swift*/XRT observations of M82 operated in the photon-counting mode are used in this work, which are retrieved from the HEASARC archive. These include a total of 106 observations spanning from 2012 April to 2015 January. 70 observations in 2014 are not used because they are badly contaminated by the supernova SN 2014J in M82. Inspection of these XRT observations confirms that X-ray photons from M82 X-1 and nearby sources dominate the field within $\sim 30'$ of M82.

2.1. Stacked images of M82 with *Swift* observations

There are three other ULXs near M82 X-1, e.g., M82 X-2, CXOU J095551.2 +694044 (here-

¹ Key Laboratory of Optical Astronomy, National Astronomical Observatories, Chinese Academy of Sciences, 20A Datun Road, Chaoyang District, Beijing 100012, China

² University of Chinese Academy of Sciences, No.19A Yuquan Road, Beijing 100049, China

³ Key Laboratory of Space Astronomy and Technology, National Astronomical Observatories, Chinese Academy of Sciences, Beijing 100012, China

[†] Send correspondence to jfliu@nao.cas.cn

after $X - 3$) and CXOU J095550.6 +694944 (hereafter X-4; Liu & Mirabel 2005; Kong et al. 2007; Strohmayer & Mushotzky 2003) with $2'' - 6''$ separations from each other. Those four ULXs can only be clearly resolved by the *Chandra X-ray observatory* (see Figure 1(a)), unfortunately there are not enough *Chandra* observations of M82 X-1 in order to perform periodicity analysis. In contrast, *Swift*/XRT has more than a hundred observations of M82 X-1, and it can marginally resolve the four ULXs in a single observation (Figure 1(b)), though the claimed half power diameter of the point spread function of XRT is $18''$. The image spatial resolution of XRT is one pixel ($2''.36$), but the positional accuracy from centroiding can be higher when there are ample photons. To reveal of all the faint and bright X-ray sources with more accurate positions, we stacked the total 106 XRT observations. Before image stacking, one pixel was equally divided into 10×10 parts, and each part (a sub-pixel) was assigned 1% of the pixel counts. Then the total 106 images in sub-pixels were matched under WCS coordinates and stacked into one (Figure 1(c)).

This stacked image (Figure 1(c)) reveals that the four ULXs are not blurred into one unresolved source, but an asymmetric structure in which X-1 and the other three ULXs are separated. X-2 is the second brightest X-ray source in M82, but it is not evident in Figure 1(c) because it is a transient and, for most of the time, it is in a quiescent state. Among the 106 *Swift* observations, only a dozen observations in which X-2 is brighter than X-3 and X-4. X-3 is also a variable X-ray source, and is visible in 46 observations. X-4 was reported as a supernova remnant candidate (Kong et al. 2007; Chiang & Kong 2011), which is supposed to have relatively constant flux.

Furthermore, to inspect whether XRT can resolve X-1 from X-3 or not, 46 observations in which X-3 is brighter than the nearby background were selected, and stacked into one image (Figure 1(d)). The rest of the 60 observations are stacked and shown in Figure 1(e). These figures imply that X-1 can be roughly resolved from X-3, while counts from X-2, X-3, and X-4 within $4''$ mix up with each other and can hardly be resolved by XRT. Thus, sources with separations larger than $4''$ can marginally resolved by XRT, but not vice versa.

2.2. Phase offset of the 62 day X-ray Period

Based on the long-term observations, *Swift*/XRT data can be used to test the 62-day modulation (KF07) of M82. Source counts were extracted from a circular region $18''$ in radius centered on X-1, with 73% of energy encircled (Moretti et al. 2005). The background was defined by a circular region with a radius of 20 pixels ($47''$) placed near M82 X-1, but avoiding the contamination from other point sources. The 0.3-10 keV background-subtracted light curve, binned per observation, was used to look for the periodicity of X-1 with the Lomb-Scargle(L-S) algorithm (Lomb 1976; Scargle 1982; ?). The power of the periodogram was normalized by the total variance of the data (Horne & Baliunas 1986). As shown in Figure 2 (a), the main peak appears at the period of 61.8 ± 2.9 days, and the error is estimated by calculating the FWHM of the main peak in the periodogram (Kovacs 1981).

The significance of the main peak in periodogram can be given by the false alarm probability (hereafter fap) as-

suming all of the datapoints were generated by stochastic noises. The fap based on the Gaussian white noise of the main peak is less than 0.001 (dashed horizontal lines in Figure 2(a)), i.e., the confidence level of this period generated by a signal instead of the white noise background is more than 99.9%. While significant peaks under the white noise background may have low significance when taking the red noise component into consideration. In contrast to white noise, whose power is independent of frequency, red noise exhibits a power-law spectrum in the form of $P(\omega) \propto f^{-\beta}$ ($\beta = 0$ for white noise), which can lead to relatively large aperiodic peaks in the power spectrum at low frequencies (Gruber et al. 2011).

In actuality, the periodogram (Figure 2(a)) does not show evidence of increasing slope for red noise at long periods, but is rather flat with a best-fit power law index of -0.32 (Vaughan 2005). In spite of this, we estimated the significance of the observed data under a red noise background. 100,000 red noise synthetic light curves with a mean and variance equal to the ones of the actual data were generated (Davies & Harte 1987; Timmer & Koenig 1995). Each synthetic light curve has the same sampling time series as the actual data set and was used to conduct L-S periodograms (see Kaaret et al. 2006 for more details). We found only two cases that power values at a period of 61.8 ± 2.9 days exceed the power (12.24) of the observed highest peak. Namely, the probability that a red noise produces a peak at the given period ranges higher than 12.24 is only 2×10^{-5} . The fap of the highest peak at the inspected frequencies (40-80 days) based on red noise is 0.0012 (confidence of 99.88%) (Charisi et al. 2015). Hence, the 62-day periodicity from *Swift*/XRT data is significant enough to be produced by a real periodic signal, and confirms the ~ 62 -day modulation of M82 discovered by KF07 with *RXTE*/PCA.

The phase shift of the 62-day period was reported by PS13 utilizing *RXTE*/PCA observations. Following the work in PS13, we folded the new *Swift*/XRT light curve (MJD 56022.9-MJD 57053.4) at 62 days to test the stability of the ~ 62 -day periodicity. The previous *RXTE* light curves from PS13 consist of two segments, which cover MJD 53250.6-54225.4 (segment 1, the same data used in KF07) and MJD 54353.8-55195.8 (segment 2), respectively. Start times of the *Swift* light curve and the two *RXTE* light curves were set to be the same (MJD 53250.6). Then the three light curves were folded at the period of 62 days (see Figure 2(b)). The two *RXTE* light curves indeed reveal a 0.4 phase offset as reported in PS13. Compared with *RXTE* light curves, the *Swift* light curve shows changes of about 0.2 in phase relative to *RXTE* segment 1, and 0.4 in phase relative to *RXTE* segment 2. It confirms the result in PS13 that the 62-day X-ray periodicity of M82 has phase changes, indicating that it is not stable.

2.3. Origin of the periodicities in M82

Since the $18''$ radius circular region used in §2.1 encircles not only X-1 but many other X-ray sources, it is not clear whether the 62-day periodicity originates from a certain single source, like X-1, or from summed contributions of several X-ray sources. Hence, we used a smaller source region with a radius of $4''$, which can separate X-1 from other X-ray sources, yet contains 30% of the energy encircled in the $18''$ region used in §2.2, to construct the

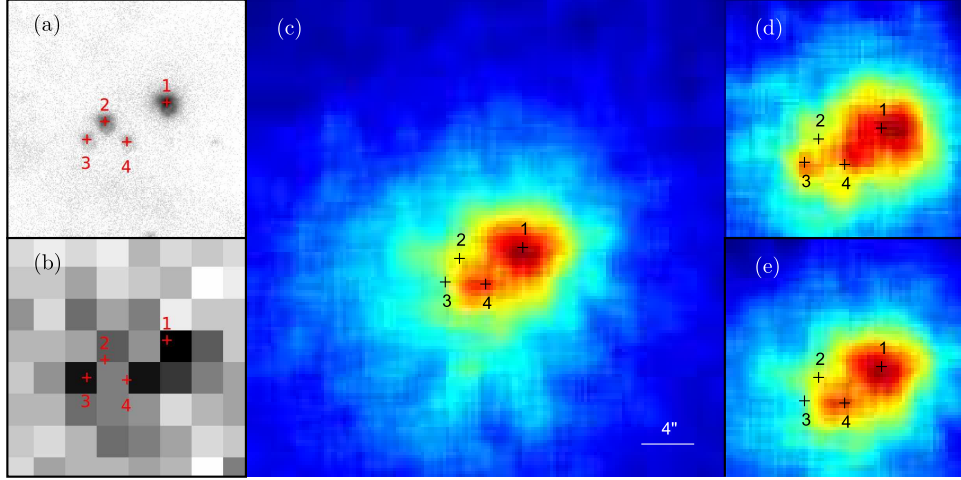


FIG. 1.— X-ray images of M82 from *Chandra*/ACIS and *Swift*/XRT. Each panel is shown on the same spatial scale, and north is up. The spatial size of (a), (b), (d), and (e) is $18'' \times 18''$, and the size of (c) is $36'' \times 36''$. The positions of X-1, X-2, X-3, and X-4 are marked by crosses and corresponding numbers. (a) *Chandra*/ACIS image from observation ObsID 5644. (b) *Swift*/XRT image from observation ObsID 00032503069, which shows that the four ULXs can be marginally resolved by *Swift*/XRT. (c) The stacked image of all 106 *Swift*/XRT observations used in this study. The counts concentrated on X-1 and X-4 reveal an asymmetric structure. (d) The stacked image of 46 *Swift*/XRT observations in which X-3 is obviously brighter than the background. (e) The stacked image of the remaining 60 observations.

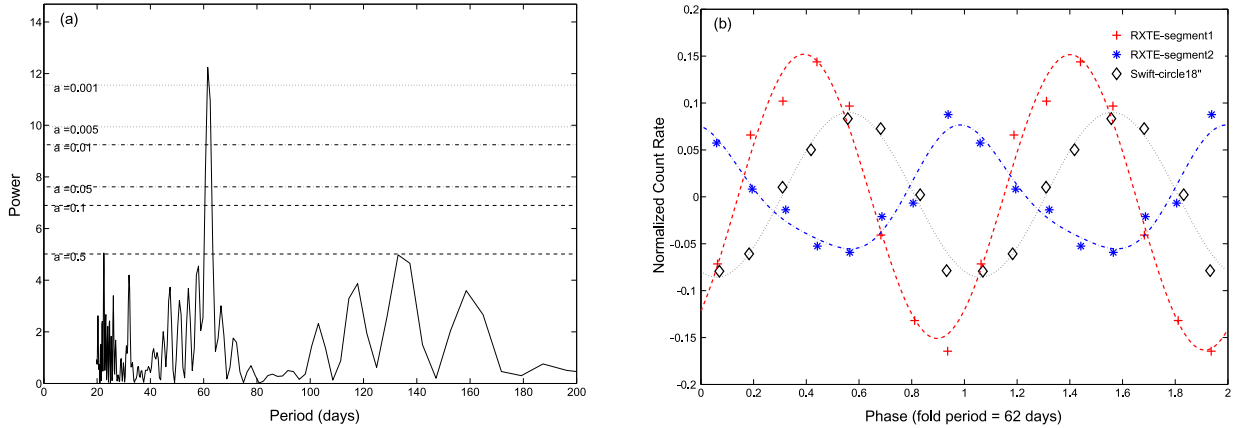


FIG. 2.— (a) L-S periodogram of a *Swift*/XRT circular region centered at X-1 with a radius of $18''$. A peak appears at 61.8 ± 2.9 days. Dashed, horizontal lines denote the fap of 0.5, 0.1, 0.05, 0.01, 0.005, and 0.001 (or confidence levels of 50%, 90%, 95%, 99%, 99.5%, and 99.9%), based on the Gaussian noise background. (b) Normalized phase light curves of *Swift*, *RXTE* segment 1, and *RXTE* segment 2 folded at 62 days. Each point is the averaged count rate of the observations falling within the given phase bin, and the error bar is shown as the standard deviation divided by the square root of the number of points in that bin. The solid sinusoidal curves are the best Fourier fit of the data.

periodicity map of M82 and analyze the origin of the 62-day modulation. We divided the region around M82 X-1 into a grid with steps of 0.5 pixel (i.e., $1''.18$) in X and Y directions, and constructed light curves with photons from the sub-pixels (as in §2.1) within a $4''$ circular region centered at each grid point. L-S periodograms were calculated as in §2.2, and the power for the strongest peak was chosen as the value for each grid point to construct the periodicity map as displayed in Figure 3(a).

This periodicity map exhibits two strong periods at 54.6 ± 2.1 days and 62.0 ± 3.3 days (denoted by the red diamond and the blue triangle, respectively, in Figure 3(a)), which are positionally coincident with X-3 and X-4 respectively. In contrast, there is almost no significant periodicity near X-1. The individual periodograms of X-1, X-2, X-3, and X-4 with source regions of $4''$ in radii are displayed in Figure 3(b). The highest peak in the periodogram of X-1 is at ~ 62.0 days, but with much lower confidence levels of 56% and 69% for white noise

and red noise background respectively. Except for X-1, the periodograms of X-2, X-3, and X-4 all show the ~ 55 -day and ~ 62 -day period, and the significance of the highest peaks in them are larger than 99% based on both white noise and red noise background. This implies that the ~ 55 - and ~ 62 -days peaks are generated by real periodic signals with high probability rather than white or red noises, and the photons from the two signals are mixed up in the region containing X-2, X-3, and X-4 (dark part in Figure 3(a)), while they still can be distinguished from the counts of X-1. Thus the 62-day periodicity is most likely associated with the region $4''$ southeast of X-1, instead of X-1 as expected.

3. DISCUSSION

By combining the *RXTE* and *Swift* light curves, we analyzed a longer term light curve. The analysis confirms phase changes of the 62-day period of M82, indicating that this period is not stable. A detailed timing analysis

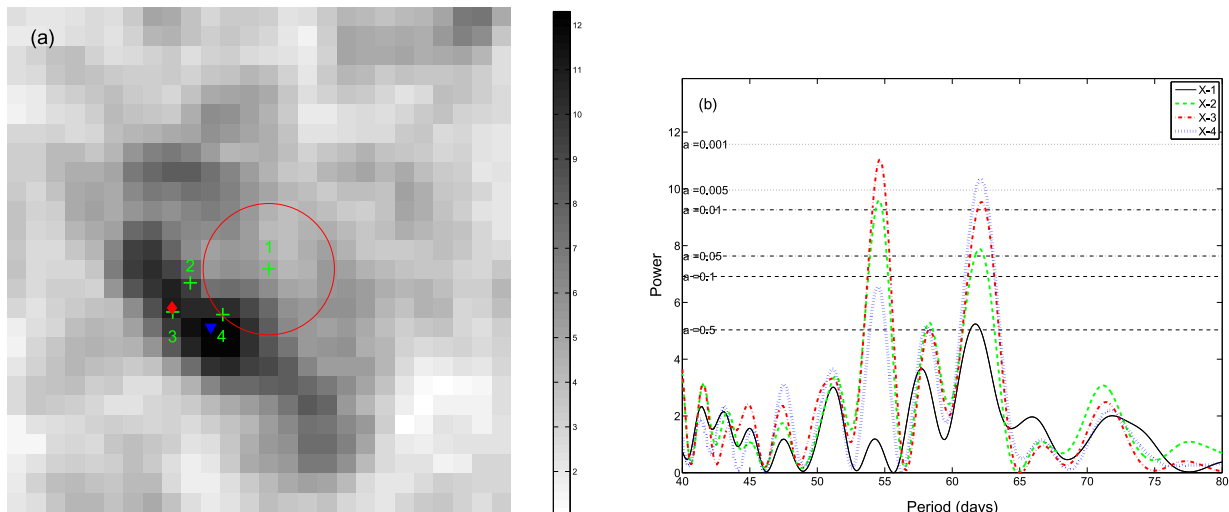


FIG. 3.— (a) Periodicity map showing the L-S periodogram maximum power for a grid with steps of 0.5 pixels (i.e., $1''.18$). The periodograms were computed with photons from subpixels within a $4''$ circular region centered at each grid point. The red circle is centered on X-1 with a radius of $4''$. The red diamond and blue triangle mark the center of the approximate 55- and 62- day periodicities respectively. It is clear that there is no significant periodicity within the $4''$ circular region of X-1. (b) L-S periodograms of X-1 (black filled line), X-2 (green line), X-3 (red line), and X-4 (blue line) extracted from source region of $4''$ in radii. It shows no significant periodicity in X-1, whereas X-2 and X-3 show two significant periodicities at ~ 55 and ~ 62 days, and X-4 shows the strongest period at 62 days. The confidence levels of the highest peaks in X-1, X-2, X-3, and X-4 based on red noise are 69%, 99.6%, 99.7%, and 99.8% respectively. Dashed, horizontal lines have the same meaning as in Figure 2 (a).

of M82 shows two significant periodicities at 55 and 62 days in a region $4''$ southeast of X-1, which contains X-2, X-3, and X-4. Given the X-ray localization precision of XRT, the periodicity map can hardly resolve X-2, X-3, and X-4 clearly, but it can easily distinguish the three ULXs from X-1. This indicates that the 62-day period is not from M82 X-1, but most likely from the three ULXs. The instability of the 62-day period may be due to the comprehensive effect of several different periodic X-ray sources, instead of a precessing accretion disk.

It is not yet clear which sources produce the ~ 55 - and ~ 62 - day periodicities. However, X-4 can be excluded first since it is a luminous young X-ray supernova remnant candidate (Kong et al. 2007; Chiang & Kong 2011), whose flux cannot fluctuate periodically. X-2 (also referred to as X42.3+59) is interpreted as a magnetized neutron star system with an orbital period of 2.5 days (Bachetti et al. 2014). Superorbital periods of neutron star binaries can range from 25 days to 160 days (Wijers & Pringle 1999). The ~ 55 days may be a superorbital period of X-2, but it may be not valid because the X-ray luminosity of X-2 is several orders of magnitude larger than for the other neutron star binaries (Matsuba et al. 1995; Reynolds et al. 1997; Orlandini et al. 1998; Suchy et al. 2008).

For X-3, it is suggested as a background active galactic nucleus because of its soft excess below 2 keV (Kong et al. 2007). However, soft excess is also common in an obscured high-mass X-ray binary (HMXB;

e.g., IGR J19140+0951 and IGR J16207-5129; Prat et al. 2008; Tomsick et al. 2009). X-3 has also been regarded as an HMXB (Mineo et al. 2012). Given the strong star-forming activities in M82, HMXBs are expected to dominate the bright X-ray sources (Chiang & Kong 2011). Assuming the isotropic unabsorbed emission, the maximum 0.5-10 keV luminosity of X-3 is 1.7×10^{40} erg s^{-1} (Kong et al. 2007), which is approximate to the (maximum-minimum) luminosity modulation of M82 ($\sim 1.6 \times 10^{40}$ erg s^{-1} ; KF07). Therefore, X-3 is bright enough to dominant the periodicity in M82 if X-3 is an HMXB with an orbital period of 62 days.

In summary, the limited spatial resolution of XRT is the bottleneck in this study, but it is already indicating that the 62-day periodicity of M82 may not come from X-1. To obtain a reliable location of the periodicities, more monitoring of M82 is needed.

We thank the anonymous referee for a number of helpful comments. We are grateful for the service of the *Swift* Data Archive. We thank Song Wang, Yu Bai, Stephan Justham and Qing Gao et al. for useful discussions. We would like to specially thank D. J. Pasham for providing *RXTE* reduced data and helpful discussions. We gratefully acknowledge support for this work from the National Science Foundation of China through grants NSFC-11333004/11425313/11473036.

REFERENCES

- Bachetti, M., Harrison, F. A., Walton, D. J., et al. 2014, *Nature*, 514, 202
 Charisi, M., Bartos, I., Haiman, Z., Price-Whelan, A. M., & Márka, S. 2015, arXiv:1502.03113
 Chiang, Y.-K., & Kong, A. K. H. 2011, *MNRAS*, 414, 1329
 Davies, R.B., & Harte, D.S. 1987, *Biometrika*, 74, 95
 Fabbiano, G. 2006, *ARA&A*, 44, 323
 Freedman, W. L., Hughes, S. M., Madore, B. F., et al. 1994, *ApJ*, 427, 628
 Gladstone, J. C., & Roberts, T. P. 2009, *MNRAS*, 397, 124
 Gruber, D., Lachowicz, P., Bissaldi, E., et al. 2011, *A&A*, 533, A61
 Horne, J. H., & Baliunas, S. L. 1986, *ApJ*, 302, 757
 Kaaret, P., Prestwich, A. H., Zezas, A., et al. 2001, *MNRAS*, 321, L29
 Kaaret, P., & Feng, H. 2007, *ApJ*, 669, 106
 Kaaret, P., Feng, H., & Gorski, M. 2009, *ApJ*, 692, 653
 Kaaret, P., Simet, M. G., & Lang, C. C. 2006, *ApJ*, 646, 174

- Kong, A. K. H., Yang, Y. J., Hsieh, P.-Y., Mak, D. S. Y., & Pun, C. S. J. 2007, *ApJ*, 671, 349
- Kovacs, G. 1981, *Ap&SS*, 78, 175
- Liu, J.-F., Bregman, J. N., Bai, Y., Justham, S., & Crowther, P. 2013, *Nature*, 503, 500
- Liu, Q. Z., & Mirabel, I. F. 2005, *A&A*, 429, 1125
- Lomb, N. R. 1976, *Ap&SS*, 39, 447
- Matsuba, E., Dotani, T., Mitsuda, K., et al. 1995, *PASJ*, 47, 575
- Matsumoto, H., Tsuru, T. G., Koyama, K., et al. 2001, *ApJ*, 547, L25
- Mineo, S., Gilfanov, M., & Sunyaev, R. 2012, *MNRAS*, 419, 2095
- Moretti, A., Campana, S., Mineo, T., et al. 2005, *Proc. SPIE*, 5898, 360
- Motch, C., Pakull, M. W., Soria, R., Gris e, F., & Pietrzyński, G. 2014, *Nature*, 514, 198
- Motta, S. E., Belloni, T. M., Stella, L., Mu oz-Darias, T., & Fender, R. 2014, *MNRAS*, 437, 2554
- Orlandini, M., Dal Fiume, D., Frontera, F., et al. 1998, *ApJ*, 500, L163
- Pasham, D. R., & Strohmayer, T. E. 2013, *ApJ*, 774, L16
- Pasham, D. R., Strohmayer, T. E., & Mushotzky, R. F. 2014, *Nature*, 513, 74
- Prat, L., Rodriguez, J., Hannikainen, D. C., & Shaw, S. E. 2008, *MNRAS*, 389, 301
- Press, W. H., Teukolsky, S. A., Vetterling, W. T., & Flannery, B. P. 1992, Cambridge: University Press, —c1992, 2nd ed.,
- Reynolds, A. P., Quaintrell, H., Still, M. D., et al. 1997, *MNRAS*, 288, 43
- Scargle, J. D. 1982, *ApJ*, 263, 835
- Strohmayer, T. E., & Mushotzky, R. F. 2003, *ApJ*, 586, L61
- Suchy, S., Pottschmidt, K., Wilms, J., et al. 2008, *ApJ*, 675, 1487
- Timmer, J., & Koenig, M. 1995, *A&A*, 300, 707
- Tomsick, J. A., Chaty, S., Rodriguez, J., et al. 2009, *ApJ*, 694, 344
- Vaughan, S. 2005, *A&A*, 431, 391
- Wijers, R. A. M. J., & Pringle, J. E. 1999, *MNRAS*, 308, 207